

**NASA Contractor Report 181830**

**ICASE REPORT NO. 89-25**

# ICASE

**NUMERICAL STUDY OF TURBULENT SECONDARY  
FLOWS IN CURVED DUCTS**

**N. Hur**

**S. Thangam**

**C. G. Speziale**

**(NASA-CR-181830) NUMERICAL STUDY OF  
TURBULENT SECONDARY FLOWS IN CURVED DUCTS  
Final Report (ICASE) 27 p CSCL 20D**

**N89-24568**

**Unclas  
G3/34 0212660**

**Contract No. NAS1-18605  
April 1989**

**INSTITUTE FOR COMPUTER APPLICATIONS IN SCIENCE AND ENGINEERING  
NASA Langley Research Center, Hampton, Virginia 23665**

**Operated by the Universities Space Research Association**



**National Aeronautics and  
Space Administration**

**Langley Research Center  
Hampton, Virginia 23665**

# NUMERICAL STUDY OF TURBULENT SECONDARY FLOWS IN CURVED DUCTS

N. Hur and S. Thangam

Department of Mechanical Engineering  
Stevens Institute of Technology  
Hoboken, New Jersey 07030

C. G. Speziale\*

Institute for Computer Applications in Science and Engineering  
NASA Langley Research Center  
Hampton, Virginia 23665

## ABSTRACT

The pressure driven, fully-developed turbulent flow of an incompressible viscous fluid in curved ducts of square cross-section is studied numerically by making use of a finite volume method. A nonlinear  $K - \epsilon$  model is used to represent the turbulence. The results for both straight and curved ducts are presented. For the case of fully-developed turbulent flow in straight ducts, the secondary flow is characterized by an eight-vortex structure for which the computed flowfield is shown to be in good agreement with available experimental data. The introduction of moderate curvature is shown to cause a substantial increase in the strength of the secondary flow and to change the secondary flow pattern to either a double-vortex or a four-vortex configuration.

---

\* This research was supported by the National Aeronautics and Space Administration under NASA Contract No. NAS1-18605 and was carried out while the author was in residence at ICASE, NASA Langley Research Center, Hampton, VA 23665.

## 1. Introduction

The study of viscous flow in curved or helically coiled ducts has been of fundamental interest to fluid dynamicists. There are numerous applications, which include the flow through turbomachinery blade passages, aircraft intakes, diffusers, and heat exchangers. Some of these problems of practical interest involve longitudinal curvature in the geometry for which the associated centrifugal forces can generate a secondary flow which is normal to the main flow direction. Such secondary flows not only cause a reduction in the volumetric flow rate, but they can also cause the axial velocity field to be distorted with an outward shift of the contours of constant velocity. In addition, it is well known that the turbulent flow in straight noncircular ducts is characterized by the occurrence of secondary flows (see Gessner and Jones 1965 and Nakayama et al, 1983). A clear understanding of the evolution and consequences of the turbulent secondary flows in curved and straight ducts is, therefore, quite important from the design standpoint. The present study is intended to address a facet of this issue, and involves the computational modeling of fully developed turbulent flow in square ducts with an emphasis on the prediction of secondary flows.

The results available in the literature on turbulent flow related to the work to be presented herein can be classified into two broad categories: fully-developed flow in straight ducts and developing flow in curved ducts. The case of fully-developed turbulent flow in straight ducts of square cross section was studied by Gessner and Jones (1965), Melling and Whitelaw (1976), and Nakayama, et al (1983), among others. Gessner and Jones (1965) conducted a series of experiments using hotwire anemometry to analyze fully-developed turbulent flow in a square duct at a Reynolds number of 150,000. They also carried out computations by a finite difference method with an algebraic stress model to predict qualitatively the major feature of the flowfield, namely, the eight-vortex secondary flow structure. Melling and Whitelaw (1976) performed detailed experiments for fully-developed flow using laser-doppler anemometry, and were the first to describe the axial velocity field and the Reynolds stress distribution in detail. Nakayama, et al (1983), on the other hand, analyzed the fully-developed flowfield in ducts of rectangular and trapezoidal cross-sections computationally using a finite-difference method based on the algebraic turbulence stress model of Launder and Ying (1972). They were able to obtain a flowfield in good agreement with the available experimental measurements for a number of selected cross-sections. Improved calculations were conducted by Gessner and Po (1977) and DeMuren and Rodi (1984), using the nonlinear algebraic stress model of Rodi.

The computational analysis of developing turbulent flow in curved square ducts has been conducted by Pratap and Spalding (1975), and by Humphrey, et al (1981). The work by Pratap and Spalding (1975) consisted of the solution of the three-dimensional time averaged Navier-Stokes equations incorporating a two-equation turbulence model based on a first order curvature ratio effect. Their study, which was conducted for a curvature ratio of 4.13 and a Reynolds number of 70,600, showed good agreement with the experimental results in the region near the entrance. However, in the fully developed region, they observed considerable discrepancies with the experimental results. Humphrey, et al (1981) also analyzed the developing turbulent flow in a square duct, but at a curvature ratio of 4.6 and a Reynolds number of 40,000. They solved the three-dimensional time-averaged Navier-Stokes equations with a two-equation turbulence model, by using a finite-difference method, and compared the results with their experimental findings obtained by laser-doppler anemometry. They concluded that in spite of the complex mean flow and Reynolds stress distributions, the cross-stream flow is controlled mainly by the centrifugal force and radial pressure gradient imbalance; consequently, the calculated mean velocity results are not strongly dependent on the turbulence model.

The present study is motivated by the lack of a detailed analysis and prediction capability for turbulent secondary flows in curved ducts. Furthermore, several of the commonly used turbulence models (in particular, the standard  $K - \epsilon$  model) are incapable of predicting the development of secondary flows in straight ducts of noncircular cross-section (see Speziale 1987). In the computational analysis to be presented, a finite-volume algorithm suitable for handling cylindrical geometry is implemented to analyze fully-developed turbulent flows in straight as well as curved square ducts using a recently developed nonlinear  $K - l$  turbulence model (Speziale 1987). In the following sections the governing equations, the development of the turbulence model, and the numerical procedure will be described in detail followed by a discussion of the results and conclusions.

## 2. The Physical Problem and Method of Solution

The problem to be considered consists of the turbulent flow of an incompressible viscous fluid in a curved duct of square cross-section. Flow in helically coiled ducts may also be analyzed in the same manner so long as the ratio of torsion to curvature remains small. The physical configuration and the coordinate system used are shown in Figure 1.

The flow is generated by a constant azimuthal pressure gradient,  $G = -\frac{1}{r} \frac{\partial \bar{P}}{\partial \theta}$  (see Figure 1). It is assumed that the flow is fully-developed so that all flow variables are independent of the

azimuthal coordinate  $\theta$ . The fully developed mean velocity field is three-dimensional, i.e. the mean (time-averaged) velocity vector  $\bar{\mathbf{v}}$  in the cylindrical coordinate system employed is of the form  $\bar{\mathbf{v}} = \bar{u}(r, z) \mathbf{e}_r + \bar{v}(r, z) \mathbf{e}_z + \bar{w}(r, z) \mathbf{e}_\theta$  where  $\mathbf{e}_r$ ,  $\mathbf{e}_z$ , and  $\mathbf{e}_\theta$  denote unit vectors in the  $r, z$  and  $\theta$  directions, respectively. Here,  $\bar{u}$  and  $\bar{v}$  represent the secondary flow while  $\bar{w}$  denotes the primary flow. The governing equations consist of the time-averaged equations for conservation of mass and momentum, and may be expressed in the following form

$$\frac{1}{r} \frac{\partial}{\partial r} (r\bar{u}) + \frac{\partial}{\partial z} (\bar{v}) = 0 \quad (1)$$

$$\begin{aligned} \frac{\partial \bar{u}}{\partial t} + \frac{1}{r} \frac{\partial}{\partial r} (r\bar{u}\bar{u}) + \frac{\partial}{\partial z} (\bar{v}\bar{u}) &= \frac{1}{r} \frac{\partial}{\partial r} \left[ r\nu \frac{\partial}{\partial r} (\bar{u}) \right] + \frac{\partial}{\partial z} \left[ \nu \frac{\partial}{\partial z} (\bar{u}) \right] \\ &\quad - \frac{1}{\rho} \frac{\partial \bar{P}}{\partial r} + \frac{\bar{w}^2}{r} - \nu \frac{\bar{u}}{r^2} \\ &\quad + \frac{1}{r} \frac{\partial}{\partial r} \left[ r \frac{\tau_{rr}}{\rho} \right] + \frac{\partial}{\partial z} \left[ \frac{\tau_{rz}}{\rho} \right] - \frac{1}{r} \frac{\tau_{\theta\theta}}{\rho} \end{aligned} \quad (2)$$

$$\begin{aligned} \frac{\partial \bar{v}}{\partial t} + \frac{1}{r} \frac{\partial}{\partial r} (r\bar{u}\bar{v}) + \frac{\partial}{\partial z} (\bar{v}\bar{v}) &= \frac{1}{r} \frac{\partial}{\partial r} \left[ r\nu \frac{\partial}{\partial r} (\bar{v}) \right] + \frac{\partial}{\partial z} \left[ \nu \frac{\partial}{\partial z} (\bar{v}) \right] \\ &\quad - \frac{1}{\rho} \frac{\partial \bar{P}}{\partial z} + \frac{1}{r} \frac{\partial}{\partial r} \left[ r \frac{\tau_{rz}}{\rho} \right] + \frac{\partial}{\partial z} \left[ \frac{\tau_{zz}}{\rho} \right] \end{aligned} \quad (3)$$

$$\begin{aligned} \frac{\partial \bar{w}}{\partial t} + \frac{1}{r} \frac{\partial}{\partial r} (r\bar{u}\bar{w}) + \frac{\partial}{\partial z} (\bar{v}\bar{w}) &= \frac{1}{r} \frac{\partial}{\partial r} \left[ r\nu \frac{\partial}{\partial r} (\bar{w}) \right] + \frac{\partial}{\partial z} \left[ \nu \frac{\partial}{\partial z} (\bar{w}) \right] \\ &\quad + \frac{G}{\rho} - \frac{\bar{u}\bar{w}}{r} - \nu \frac{\bar{w}}{r^2} \\ &\quad + \frac{1}{r} \frac{\partial}{\partial r} \left[ r \frac{\tau_{r\theta}}{\rho} \right] + \frac{\partial}{\partial z} \left[ \frac{\tau_{z\theta}}{\rho} \right] + \frac{1}{r} \frac{\tau_{r\theta}}{\rho} \end{aligned} \quad (4)$$

where  $G = -\frac{1}{r} \frac{\partial \bar{P}}{\partial \theta}$  is the azimuthal mean pressure gradient which is held constant,  $\rho$  is the fluid density, and  $\nu$  is the kinematic viscosity of the fluid which can be neglected for high Reynolds number turbulent flows. The components of the Reynolds stress tensor  $\tau_{ij}$  appearing in (3) can be obtained through various modeling techniques such as algebraic, one-equation, two-equation, and second-order closure models (Launder and Spalding 1972 and Lumley 1978). Recently, a nonlinear two-equation model of the  $K-l$  and  $K-\epsilon$  type was developed by Speziale (1987). This model yields more accurate predictions for normal Reynolds stress anisotropies allowing

for the calculation of turbulent secondary flows. The nonlinear  $K - l$  model takes the form:

$$\begin{aligned} \tau_{ij} = & -\frac{2}{3}\rho K \delta_{ij} + \rho K^{1/2} l \bar{S}_{ij} + C_D \rho l^2 \left( \bar{S}_{im} \bar{S}_{mj} - \frac{1}{3} \bar{S}_{mn} \bar{S}_{mn} \delta_{ij} \right) \\ & + C_E \rho l^2 \left( \overset{\circ}{\bar{S}}_{ij} - \frac{1}{3} \overset{\circ}{\bar{S}}_{mm} \delta_{ij} \right) \end{aligned} \quad (5)$$

where

$$\bar{S}_{ij} = \frac{1}{2} \left( \frac{\partial \bar{v}_i}{\partial x_j} + \frac{\partial \bar{v}_j}{\partial x_i} \right) \quad (6)$$

$$\overset{\circ}{\bar{S}}_{ij} = \frac{\partial \bar{S}_{ij}}{\partial t} + \bar{\mathbf{v}} \cdot \nabla \bar{S}_{ij} - \frac{\partial \bar{v}_i}{\partial x_k} \bar{S}_{kj} - \frac{\partial \bar{v}_j}{\partial x_k} \bar{S}_{ki} \quad (7)$$

are the mean rate of strain tensor and its frame-indifferent Oldroyd derivative, respectively;  $K$  is the turbulent kinetic energy, and  $l$  is the turbulent length scale.  $C_D$  and  $C_E$  are dimensionless constants that each assume the value of 1.68 which was obtained by Speziale (1987) from correlations with turbulent channel flow data. The turbulent length scale  $l$  can be prescribed algebraically by empirical means, or can be tied to the turbulent kinetic energy  $K$  and dissipation rate  $\epsilon$  through the relation

$$l = 2C_\mu \frac{K^{3/2}}{\epsilon} \quad (8)$$

where  $C_\mu$  is a dimensionless constant which is typically taken to be 0.09. This forms the basis for the nonlinear  $K - \epsilon$  model for which (5) - (7) are supplemented with modeled transport equations for  $K$  and  $\epsilon$  that take the form

$$\frac{\partial K}{\partial t} + \bar{v}_i \frac{\partial K}{\partial x_i} = \frac{\partial}{\partial x_i} \left( \frac{C_\mu K^2}{\sigma_k \epsilon} \frac{\partial K}{\partial x_i} \right) + \tau_{ij} \frac{\partial \bar{v}_i}{\partial x_j} - \epsilon \quad (9)$$

$$\frac{\partial \epsilon}{\partial t} + \bar{v}_i \frac{\partial \epsilon}{\partial x_i} = \frac{\partial}{\partial x_i} \left( \frac{C_\mu K^2}{\sigma_\epsilon \epsilon} \frac{\partial \epsilon}{\partial x_i} \right) + C_{\epsilon 1} \frac{\epsilon}{K} \tau_{ij} \frac{\partial \bar{v}_i}{\partial x_j} - C_{\epsilon 2} \frac{\epsilon^2}{K} \quad (10)$$

where  $\sigma_k$ ,  $\sigma_\epsilon$ ,  $C_{\epsilon 1}$  and  $C_{\epsilon 2}$  are dimensionless constants that are usually taken to be 1.0, 1.3, 1.44, and 1.92, respectively. The standard  $K - \epsilon$  model is obtained in the limit as  $C_D, C_E \rightarrow 0$ .

Weaknesses in the performance of the modeled transport equations (9) - (10) for  $K$  and  $\epsilon$  have been pointed out numerous times in the literature for problems involving swirl and streamline curvature (see Pope 1978 and Reynolds 1987). However, several attempts at developing improved versions of these modeled transport equations has not met with much success. It is a difficult problem that requires a substantial research effort to fully resolve. In this paper, we

want to examine the efficacy of the nonlinear Reynolds stress correction to the K -  $l$  and K -  $\epsilon$  models given by equation (5), for problems involving secondary flows with streamline curvature. Hence, we will specify K and  $l$  empirically, based on experimental data for turbulent flow in rectangular channels, in order to determine the predictive capability of the nonlinear correction to the Reynolds stress independent of the deficiencies in the modeled transport equations for K and  $\epsilon$ .

For fully-developed turbulent flow in a curved duct (using the cylindrical coordinate system shown in Figure 1), the components of the Reynolds stress tensor corresponding to the nonlinear K -  $l$  model (5) can be approximated as follows:

$$\begin{aligned} \tau_{rr} = & -\frac{2}{3}\rho K + \rho K^{1/2} l \frac{\partial \bar{u}}{\partial r} + C_D \rho l^2 \left[ \frac{1}{12} \left\{ r \frac{\partial}{\partial r} \left( \frac{\bar{w}}{r} \right) \right\}^2 - \frac{1}{6} \left\{ \frac{\partial \bar{w}}{\partial z} \right\}^2 \right] \\ & + C_E \rho l^2 \left[ \frac{1}{3r} \frac{\partial}{\partial r} (r^2 \bar{w}) \frac{\partial}{\partial r} \left( \frac{\bar{w}}{r} \right) + \frac{1}{3} \left( \frac{\partial \bar{w}}{\partial z} \right)^2 \right] \end{aligned} \quad (11)$$

$$\begin{aligned} \tau_{zz} = & -\frac{2}{3}\rho K + \rho K^{1/2} l \frac{\partial \bar{v}}{\partial z} + C_D \rho l^2 \left[ -\frac{1}{6} \left\{ r \frac{\partial}{\partial r} \left( \frac{\bar{w}}{r} \right) \right\}^2 + \frac{1}{12} \left\{ \frac{\partial \bar{w}}{\partial z} \right\}^2 \right] \\ & + C_E \rho l^2 \left[ \frac{1}{3} \left\{ r \frac{\partial}{\partial r} \left( \frac{\bar{w}}{r} \right) \right\}^2 + \frac{1}{3} \left( \frac{\partial \bar{w}}{\partial z} \right)^2 \right] \end{aligned} \quad (12)$$

$$\begin{aligned} \tau_{\theta\theta} = & -\frac{2}{3}\rho K + \rho K^{1/2} l \frac{\bar{u}}{r} + C_D \rho l^2 \left[ \frac{1}{12} \left\{ r \frac{\partial}{\partial r} \left( \frac{\bar{w}}{r} \right) \right\}^2 + \frac{1}{12} \left\{ \frac{\partial \bar{w}}{\partial z} \right\}^2 \right] \\ & + C_E \rho l^2 \left[ -\frac{2}{3} r^{1/2} \frac{\partial}{\partial r} \left\{ r^{1/2} \bar{w} \right\} \frac{\partial}{\partial r} \left( \frac{\bar{w}}{r} \right) - \frac{2}{3} \left( \frac{\partial \bar{w}}{\partial z} \right)^2 \right] \end{aligned} \quad (13)$$

$$\tau_{r\theta} = \tau_{\theta r} = \rho K^{1/2} \frac{l}{2} r \frac{\partial}{\partial r} \left( \frac{\bar{w}}{r} \right) \quad (14)$$

$$\begin{aligned} \tau_{rz} = \tau_{zr} = & \rho K^{1/2} \frac{l}{2} \left( \frac{\partial \bar{u}}{\partial z} + \frac{\partial \bar{v}}{\partial r} \right) + C_D \rho l^2 \left[ \frac{1}{4} r \frac{\partial}{\partial r} \left( \frac{\bar{w}}{r} \right) \frac{\partial \bar{w}}{\partial z} \right] \\ & + C_E \rho l^2 \left[ -\frac{1}{2} \frac{\bar{w}}{r} \frac{\partial \bar{w}}{\partial z} \right] \end{aligned} \quad (15)$$

$$\tau_{z\theta} = \tau_{\theta z} = \rho K^{1/2} \frac{l}{2} \frac{\partial \bar{w}}{\partial z} \quad (16)$$

(see Hur 1988 for more details). In deriving (11)-(16), terms that are quadratic in the secondary flow velocity components  $\bar{u}, \bar{v}$  have been neglected since they are small (i.e.,  $\|\bar{u}, \bar{v}\|/\|\bar{w}\| < 0.1$  for the computations to be presented herein where  $\|\cdot\|$  denotes the maximum norm). As alluded to earlier, the turbulent kinetic energy K and length scale  $l$  will be specified empirically based

on the experimental data of Laufer (1951) for turbulent channel flow (i.e., for turbulent flow in a large-aspect-ratio rectangular duct). It will now be shown that the data of Laufer can be represented by the power law

$$\frac{K^{1/2}}{U_0} = b_k \left( \frac{Sd}{U_0} \right)^{a_k} \quad (17)$$

$$\frac{l}{d} = b_l \left( \frac{Sd}{U_0} \right)^{a_l} \quad (18)$$

in the interior of the duct where  $U_0$  is the centerline mean velocity,  $d$  is the half-width of the duct, and  $a_k$ ,  $a_l$ ,  $b_k$ , and  $b_l$  are dimensionless constants. In (17) - (18),  $S$  is the mean strain rate defined by

$$S = (\bar{S}_{ij} \bar{S}_{ij})^{1/2} \quad (19)$$

In Figures 2 - 3, the turbulent kinetic energy and length scale are shown as a function of the mean strain rate for three different Reynolds numbers. For the following choice of empirical constants:

$$a_k = \begin{cases} 0, & Sd/U_0 < 0.06 \\ 0.43, & 0.06 \leq Sd/U_0 < 0.3 \\ 0, & Sd/U_0 \geq 0.3 \end{cases} \quad (20)$$

$$b_k = \begin{cases} 0.032, & Sd/U_0 < 0.06 \\ 0.11, & 0.06 \leq Sd/U_0 < 0.3 \\ 0.064, & Sd/U_0 \geq 0.3 \end{cases} \quad (21)$$

$$a_l = \begin{cases} 0, & Sd/U_0 < 0.04 \\ -0.33, & 0.04 \leq Sd/U_0 < 0.25 \\ -0.90, & Sd/U_0 \geq 0.25 \end{cases} \quad (22)$$

$$b_l = \begin{cases} 0.18, & Sd/U_0 < 0.04 \\ 0.063, & 0.04 \leq Sd/U_0 < 0.25 \\ 0.028, & Sd/U_0 \geq 0.25 \end{cases} \quad (23)$$

the power laws (17) - (18) do a reasonably good job in collapsing the experimental data for a variety of Reynolds numbers as shown in Figures 2 - 3. These power laws are reminiscent

of the ones used in viscoelastic flows; of course, the qualitative similarities between the mean turbulent flow of a Newtonian fluid and the laminar flow of a non-Newtonian fluid have long been recognized (see Lumley 1970). They have the advantage of allowing for a *substantial reduction in the level of computation* since separate transport equations for  $K$  and  $\epsilon$  do not have to be solved. Furthermore, they provide a more accurate measure of  $K$  and  $l$  for straight ducts than that which can be obtained from modeled transport equations for  $K$  and  $\epsilon$  (this allows for the study of the performance of the nonlinear Reynolds stress model in isolation from the complicating factor of defects in the  $K$  and  $\epsilon$  modeled transport equations). Although these power laws become less accurate for curved duct flows, the errors introduced are moderately small for mild curvatures and are no worse than those that arise from the standard modeled transport equations for  $K$  and  $\epsilon$ .

The boundary conditions for the secondary flow velocities  $\bar{u}$  and  $\bar{v}$  are set equal to zero at the duct walls. In order to avoid resolving the very steep gradients of the azimuthal mean velocity  $\bar{w}$  near the wall for turbulent flows, wall functions are used. These wall functions are based conventionally on a production equals dissipation equilibrium hypothesis and the law of the wall for the mean velocity profile, (c.f. Amano 1984 for more details). The boundary conditions for the pressure are obtained in the usual fashion (c.f. Patankar 1980). The mean strain rate is approximated by

$$S = \left[ \frac{1}{2} \left\{ \frac{\partial}{\partial r} \left( \frac{\bar{w}}{r} \right) \right\}^2 + \frac{1}{2} \left( \frac{\partial \bar{w}}{\partial z} \right)^2 \right]^{1/2} \quad (24)$$

which is obtained by neglecting quadratic terms in the mean secondary flow.

A finite volume scheme is used to solve the Reynolds equations (1) - (4), with the nonlinear  $K - l$  model given by equations (11) - (16). The method of solution closely follows that outlined by Patankar (1980) as modified for the cylindrical coordinate system which is used in conjunction with the curved duct geometry. In this procedure, the physical domain is discretized into a finite number of computational cells (see Figure 4). At the centroid of each (i.e., at point  $p$ ), variables such as the pressure and azimuthal component of the mean velocity are defined; the components of the mean velocity responsible for transport in the cross-sectional planes are defined at the cell boundaries. The difference equations for all of the variables are then obtained by integration over a control volume. A detailed description of the procedure used for obtaining these equations may be found in Hur (1988).

In the present work, the system of algebraic equations which result from the differencing procedure used for the governing equations (1) - (4) are solved by a successive line under relaxation (SLUR) procedure with the repeated use of the tridiagonal matrix algorithm (Isaacson & Keller 1970). The details of the solution procedure and the algorithm development are given elsewhere (Hur 1988). The following steps constitute only a brief summary of the technique:

- (a) A set of pseudo-velocity components (for the secondary flow velocity) are obtained from the discretized momentum equations by assuming uniform pressure in the computational domain.
- (b) These pseudo-velocities are then used to obtain the pressure by solving the discretized equation for the conservation of mass with the SLUR method.
- (c) Based on the pressure obtained in (b), the secondary flow velocity components are obtained from the discretized momentum equations with the SLUR method.
- (d) The correction for the velocity components are obtained by evaluating the correction for the mass flux in each cell.
- (e) Using the corrected velocities from (d), the axial velocity is obtained by the SLUR method.
- (f) The values of kinetic energy and length scale are then computed using the corrected velocity field.
- (g) The procedure is repeated with the updated values of the variables until adequate convergence is obtained.

In addition, a time-averaged stream function  $\bar{\psi}$  for the secondary flow can be defined in the following manner

$$\bar{u} = -\frac{1}{r} \frac{\partial \bar{\psi}}{\partial z} \quad (25)$$

$$\bar{v} = \frac{1}{r} \frac{\partial \bar{\psi}}{\partial r} \quad (26)$$

and can be obtained from the mean velocity field for analyzing the secondary flowfield. In the following section the results obtained by the computational technique outlined herein is discussed and compared with available experimental and computational findings.

### 3. Results and Discussion

The model predictions for turbulent flow in a straight duct will be analyzed first, followed by flow in curved ducts. The experimental investigations on turbulent duct flow include the works of Gessner & Jones (1965), Brundrett & Baines (1964), Launder & Ying (1972), and

Melling & Whitelaw (1976) among others. In the present work, computations were performed at a Reynolds number of about 42,000 in ducts of square cross-section. This was done to facilitate comparison with the results of Melling & Whitelaw (1976), since their experiments were performed at the same Reynolds number and include laser anemometer measurements of the flow pattern with a detailed documentation of the Reynolds stress components. It should be noted here that Melling & Whitelaw (1976) did not evaluate the secondary flow stream function; these are obtained from other sources, although at different Reynolds numbers (e.g., Gessner & Jones 1965; Nakayama, et al 1983).

The time-averaged secondary flow streamlines for the straight duct of square cross-section is shown in Figure 5. It should be noted that the flow is outward towards the corner and returns to the center along the wall thus forming eight counter-rotating vortices. Qualitative comparisons with the experimental results of Gessner & Jones (1965) for a Reynolds number of 150,000 and the computational results of Nakayama, et al (1983) for a Reynolds number of 83,000 are possible as shown in Figure 5. The computations by Nakayama, et al (1983) are based on the algebraic stress model developed by Launder & Ying (1972). It can be seen here that the present model agrees with the experimental results of Gessner and Jones (1965) in the sense that it also exhibits weaker secondary flow velocities near the center of the duct.

Due to the secondary flow associated with the turbulence, the axial velocity profile for  $\bar{w}$  is distorted, as shown in Figure 6. Comparison with the experiments of Melling & Whitelaw (1976) is also shown in Figure 6 and the results indicate qualitatively good agreement. The computed values of the Reynolds shear stress will now be compared with the experiments. The results for the two shear stress components,  $\tau_{xz}$  and  $\tau_{yz}$  (where  $x$  and  $y$  are the horizontal and vertical coordinates in the plane of the secondary flow and  $z$  is the coordinate normal to this plane) are shown in Figures 7 – 8. As can be seen from these results, the computed values of  $\tau_{xz}$  and  $\tau_{yz}$  are in good agreement with the experimental findings.

The computations were then extended to flow in curved ducts. Figures 9(a) - (d) show the evolution of the flow field as the curvature ratio  $C_r$  (i.e., the ratio of the radius of curvature to the duct width) increases for a Reynolds number of about 42,000. In the case of curved ducts, the interaction between the centrifugal force and the force induced by the normal Reynolds stress differences (due to the anisotropic turbulence) characterizes the secondary flow. However, as can be seen from Figures 9(a) - (b), even for very loosely coiled ducts (i.e., ducts of large curvature ratio) the fully developed flow field is characterized by a predominately double vortex structure

which is representative of a flow field dominated by centrifugal effects. There is, however, a pair of weak counter-rotating vortices near the outer wall of the duct. When the curvature ratio is decreased (i.e., as the duct is coiled tighter), the centrifugal effects gain further dominance, and the vortices near the outer wall and, hence, the secondary flow gain strength and assume a four-vortex structure as shown in Figures 9(c) - (d). The effect of an increase in the secondary flow intensity on the azimuthal velocity profiles can also be observed in Figures 9(a) - (d). As can be seen from the constant velocity lines, there is a substantial outward shift of the azimuthal velocity field with a decrease in the curvature ratio.

In Figure 10, the associated increase in the secondary flow intensity with a decrease in the curvature ratio (i.e., increase in duct curvature) is shown. From this figure, it is clear that curvature can increase the secondary flow intensity (defined as  $|\bar{u}, \bar{v}|_{max}/\bar{w}_{max}$ ) from 0.02 to 0.10.

#### 4. Conclusion

A numerical study of turbulent secondary flows in straight and curved ducts of square cross section has been conducted using the nonlinear K -  $l$  model of Speziale (1987). The results are shown to compare well with the detailed laser-Doppler anemometry measurements of Melling & Whitelaw (1976) for fully-developed turbulent flow in straight ducts of square cross-section. Here, the model predicts an eight vortex secondary flow consistent with experimental observations. For curved ducts, the model predicts a double vortex secondary flow for mild to moderate curvature and a four-vortex secondary flow for moderate to strong curvature. These regimes are analogous to those that are observed in laminar curved duct flows (c.f. Cheng, Lin and Ou 1976) with one major exception: for the laminar case there would be no secondary flows in straight ducts (i.e., in the limit as  $C_r \rightarrow \infty$ ).

In our opinion, the calculations presented in this study indicate that the nonlinear K -  $l$  and K -  $\epsilon$  model has the promise to yield more accurate predictions for curved turbulent flows than the more standardly used eddy viscosity models. This nonlinear two-equation model could provide a useful alternative to a second-order closure model for those applications where savings in computational expense is a high priority. Future research should be directed toward the generation of a full nonlinear K -  $\epsilon$  model solution to the curved flow problem. Invariably, this will require a careful examination of the modeled dissipation rate transport equation to properly account for curvature effects. With such improvements, the nonlinear K -  $\epsilon$  model could have a variety of important technological applications to turbulent flows involving streamline curvature.

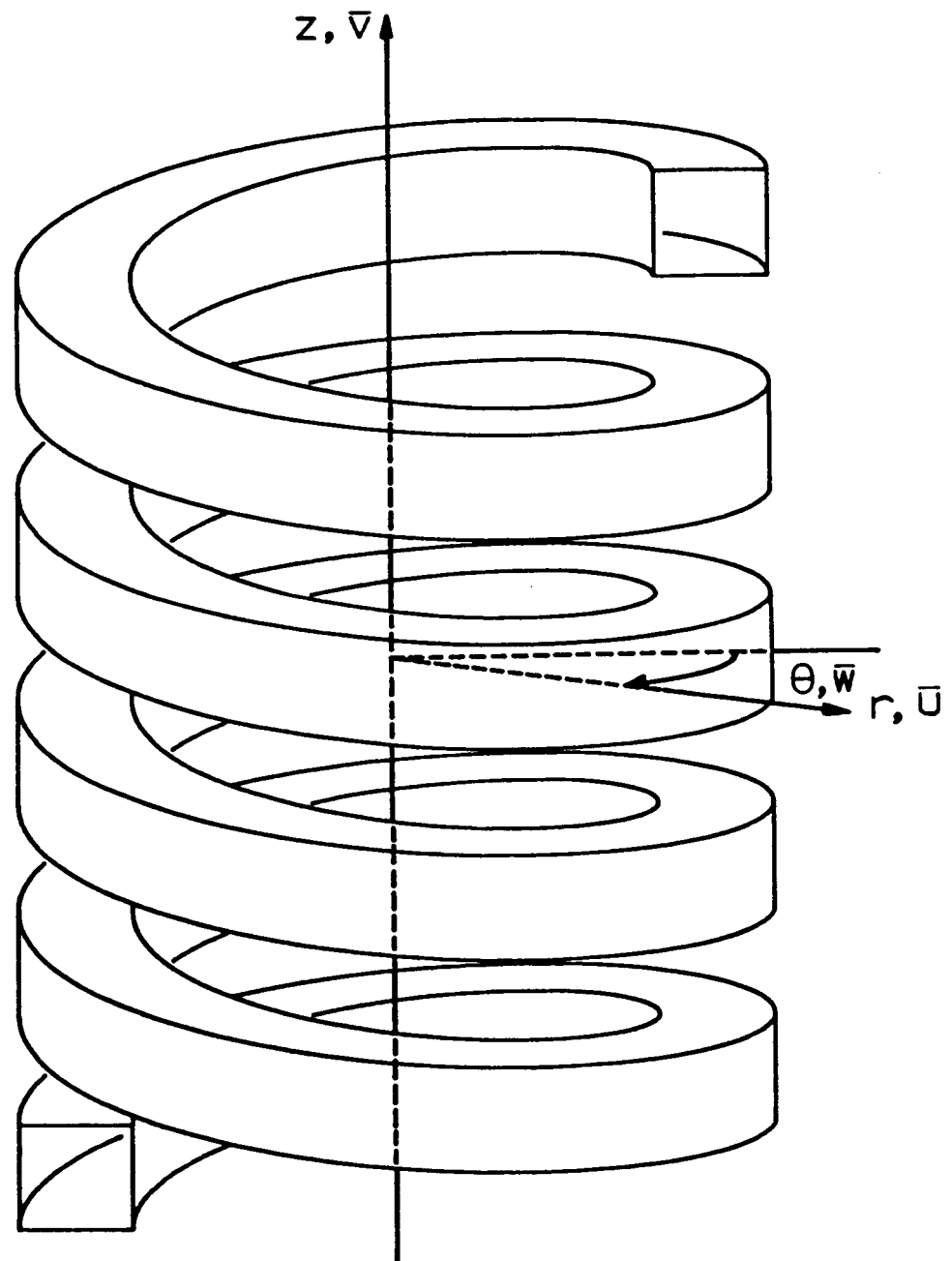
## References

- Amano, R.S. 1984 "Development of a Turbulent Near-Wall Model and its Application to Separated and Reattached Flow," *Numerical Heat Transfer*, Vol. 7, 59–75.
- Brundrett, E. & Baines, W.D. 1964 "The Production and Diffusion of Vorticity in Duct Flow," *Journal of Fluid Mechanics*, Vol. 19, 375–394.
- Cheng, K. C., Lin, R. C., and Ou, J. W. 1976 "Fully-Developed Laminar flow in Curved Rectangular Channels," *ASME J. Fluids Engng.*, Vol. 98, 41–48.
- DeMuren, A. and Rodi, W. 1984 "Calculation of Turbulence-Driven Secondary Motion in Non-Circular Ducts." *J. Fluid Mech.*, Vol. 140, 189–222.
- Gessner, F. B. & Jones, J. B. 1965 "On Some Aspects of Fully-Developed Turbulent Flow in Rectangular Channels," *Journal of Fluid Mechanics*, Vol. 23, 689–713.
- Gessner, F. B. and Po, J. K. 1977 "A Reynolds Stress Model for Turbulent Corner Flows-Part II: Comparisons Between Theory and Experiment." *ASME J. Fluids Engineering*, Vol. 99, pp. 269–277.
- Humphrey, J. A. C., Whitelaw, J. H., & Yee, G. 1981 "Turbulent Flow in a Square Duct with Strong Curvature," *Journal of Fluid Mechanics*, Vol. 103, 443–463.
- Hur, N., 1988 "Numerical Study of Secondary Flows in Curved Ducts." Ph.D. Thesis, Stevens Institute of Technology.
- Isaacson, E. & Keller, H. B. 1970 *Analysis of Numerical Methods*, Wiley.
- Laufer, J. 1951 "Investigation of Turbulent Flow in a Two-Dimensional Channel," *NACA TN 1053*.
- Launder, B. E. & Spalding, D. B. 1972 *Mathematical Models of Turbulence*, Academic Press.
- Launder, B. E. & Ying, W. M. 1972 "Secondary Flows in Ducts of Square Cross-Section," *Journal of Fluid Mechanics*, Vol. 54, 289–295.
- Lumley, J. L. 1970 "Toward a Turbulent Constitutive Relation," *Journal of Fluid Mechanics*, Vol. 41, 413–434.
- Lumley, J. L. 1978 "Turbulence Modeling," *Adv. Appl. Mech.*, Vol. 18, 123–176.

- Majumdar, A. K., Pratap, V. S., & Spalding, D. B. 1977 "Numerical Computation of Flow in Rotating Ducts," *ASME J. of Fluids Engineering*, Vol. 99, 148–153.
- Melling, A. & Whitelaw, J. H. 1976 "Turbulent Flow in a Rectangular Duct," *Journal of Fluid Mechanics*, Vol. 78, 289–315.
- Nakayama, A., Chow, W. L., & Sharma, D. 1983 "Calculation of Fully Developed Turbulent Flows in Ducts of Arbitrary Cross-Section," *Journal of Fluid Mechanics*, Vol. 128, 199–217.
- Patankar, S. V. 1980 *Numerical Heat Transfer and Fluid Flow*, McGraw-Hill.
- Pope, S. B. 1978 "An Explanation of the Turbulent Round-Jet/Plane-Jet Anomaly." *AIAA J.* Vol. 16, pp. 279–281.
- Pratap, V. S. & Spalding, D. B. 1975 "Numerical Computation of the Flow in Curved Ducts," *Aeronautical Quarterly* Vol. 26, 219–228.
- Reynolds, W. C. 1987 "Fundamentals of Turbulence for Turbulence Modeling and Simulation." *Lecture Notes for Von Karman Institute, AGARD Lecture Series No. 86*, North Atlantic Treaty Organization.
- Roache, P. J. 1972 *Computational Fluid Dynamics*, Hermosa.
- Speziale, C. G. 1987 "On Nonlinear  $K - l$  and  $K - \epsilon$  Models of Turbulence," *Journal of Fluid Mechanics*, Vol. 178, 459–475.

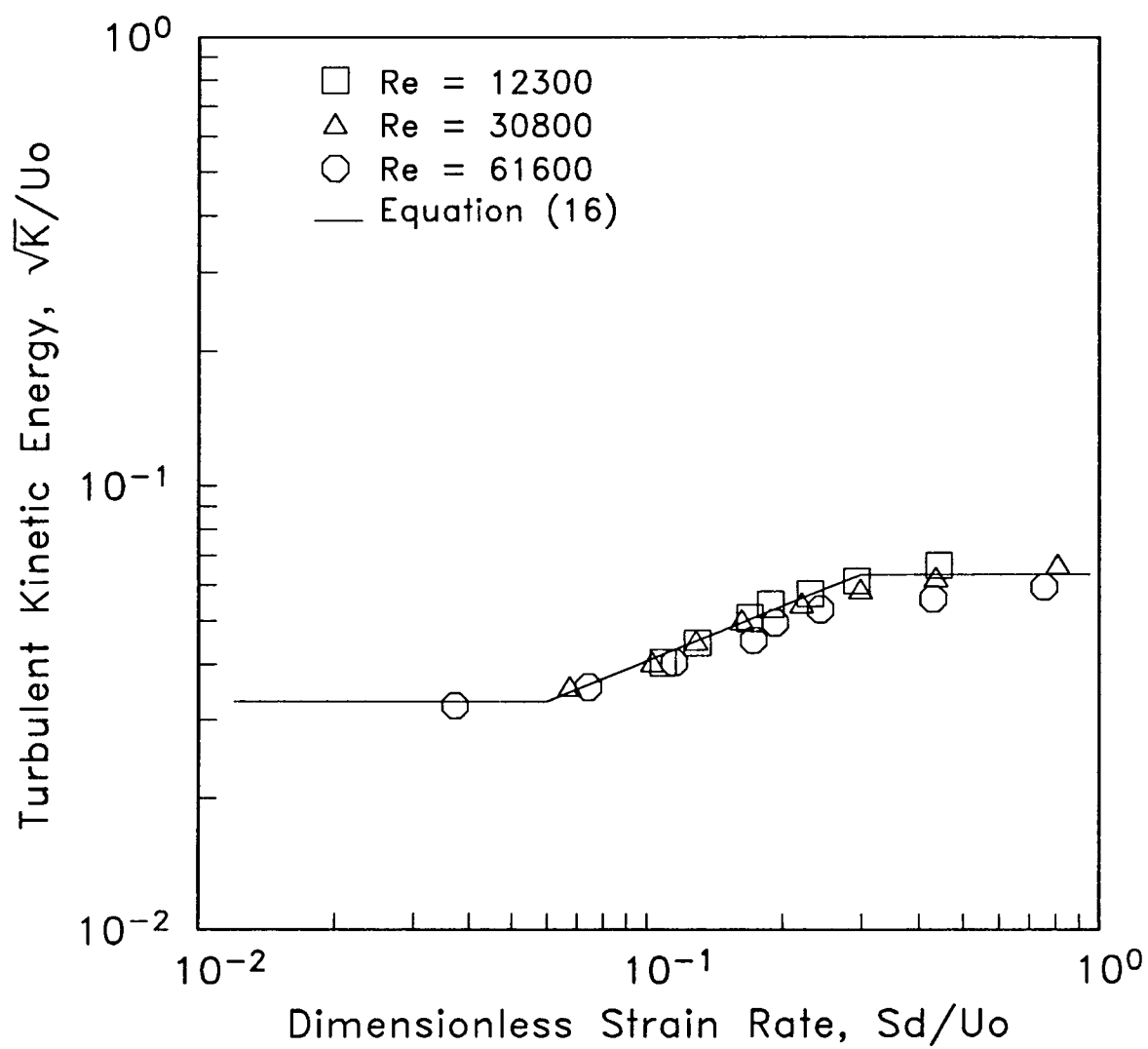
## List of Figures

- Figure 1 Physical Configuration and Coordinate System of a Helically Coiled Duct.
- Figure 2 Kinetic Energy as a Function of Strain Rate Based on the Data of Laufer (1951).
- Figure 3 Length Scale of Turbulence as a Function of Strain Rate Based on the Data of Laufer (1951).
- Figure 4 Computational Domain Illustrating the Staggered Mesh System.
- Figure 5 Comparison of Fully-Developed Secondary Flow Streamlines based on the Non-linear K- $l$  Model in a Straight Duct at  $Re \approx 42000$  with the Experiments of Gessner & Jones (Curve A:  $Re \approx 150000$ ) and the Computations of Nakayama (Curve B:  $Re \approx 83000$ ).
- Figure 6 Comparison of Azimuthal Velocity Contours ( $\bar{w}$ ) at  $Re \approx 42000$ :  
—— Nonlinear K- $l$  Model; ----- Experiments of Melling & Whitelaw.
- Figure 7 Comparison of Reynolds Stress ( $\tau_{xz}$ ) Contours at  $Re \approx 42000$ :  
—— Nonlinear K- $l$  Model; ----- Experiments of Melling & Whitelaw.
- Figure 8 Comparison of Reynolds Stress ( $\tau_{yz}$ ) Contours at  $Re \approx 42000$ :  
—— Nonlinear K- $l$  Model; ----- Experiments of Melling & Whitelaw.
- Figure 9 Secondary Flow Streamlines ( $\bar{\psi}$ ) and Azimuthal Velocity Contours ( $\bar{w}$ ) for Turbulent Flow in Curved Ducts at  $Re \approx 42000$  for Different Curvature Ratios. (a)  $Cr = 125$  (b)  $Cr = 62.5$  (c)  $Cr = 31.25$  (d)  $Cr = 15.63$
- Figure 10 Effect of Curvature Ratio on Secondary Flow Intensity at  $Re \approx 42000$ .



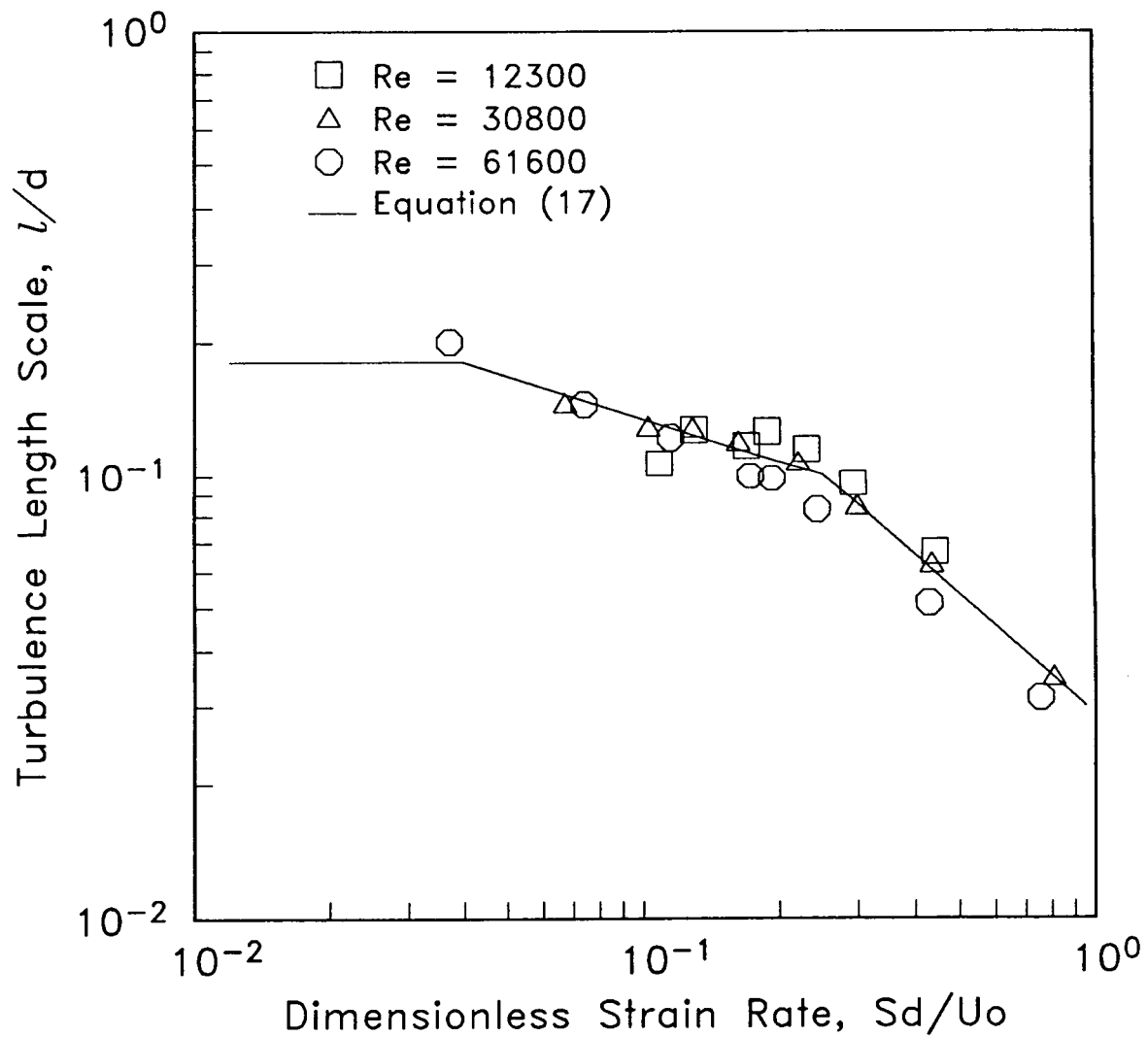
**Physical Configuration and Coordinate System**

**Figure 1**



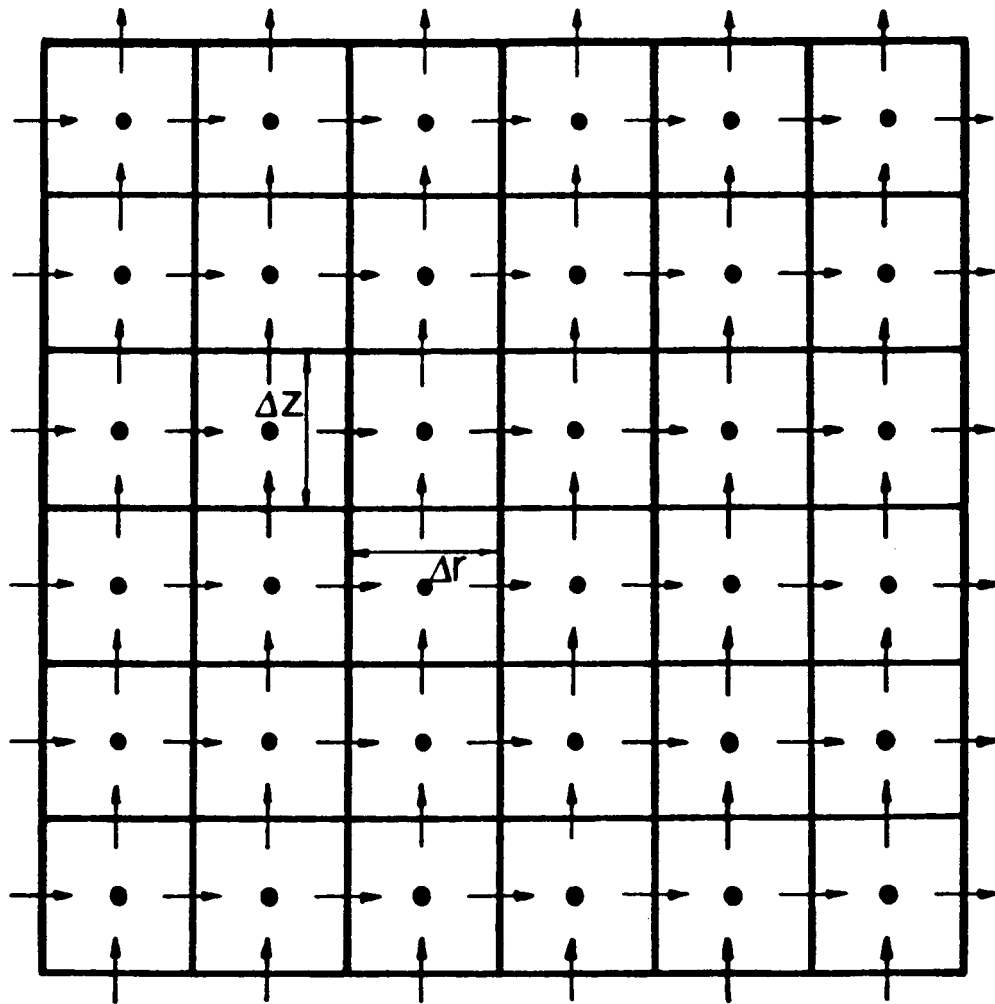
Kinetic Energy as a Function of Strain Rate  
[Data of Laufer (1951)]

**Figure 2**



Turbulence Length Scale as a Function of Strain Rate  
[Data of Laufer (1951)]

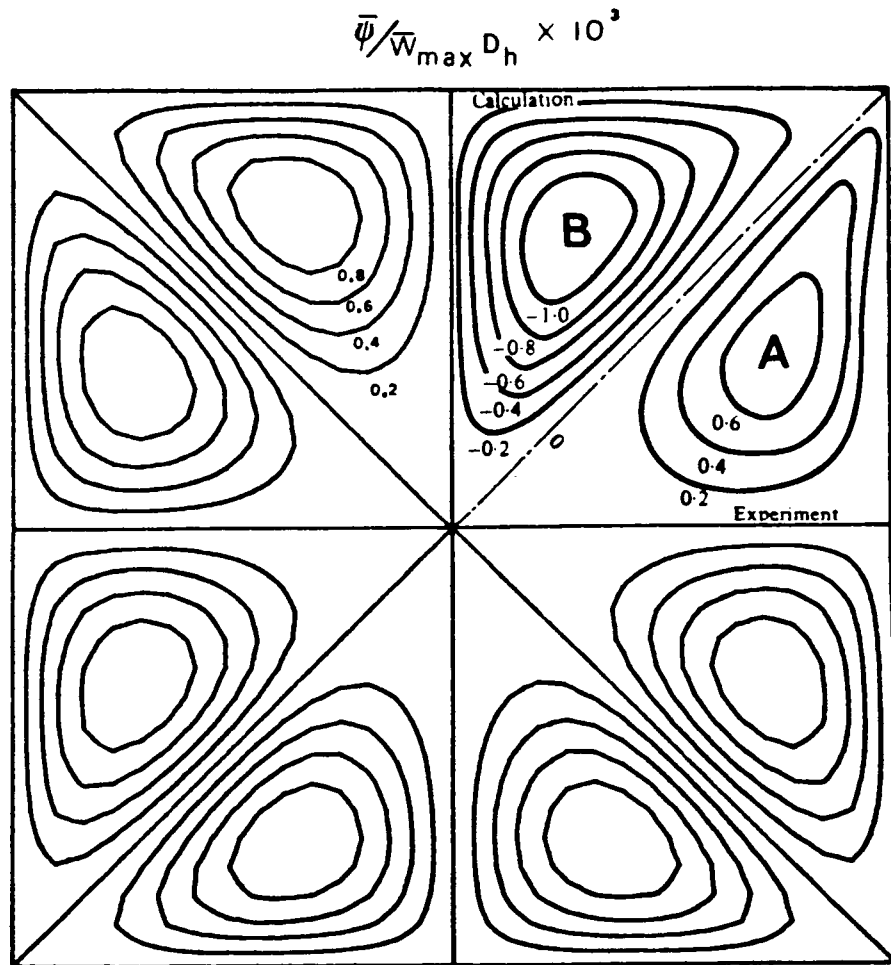
**Figure 3**



$\rightarrow \bar{u}, \uparrow \bar{v}, \bullet \bar{w}, \bar{p}, K, l$

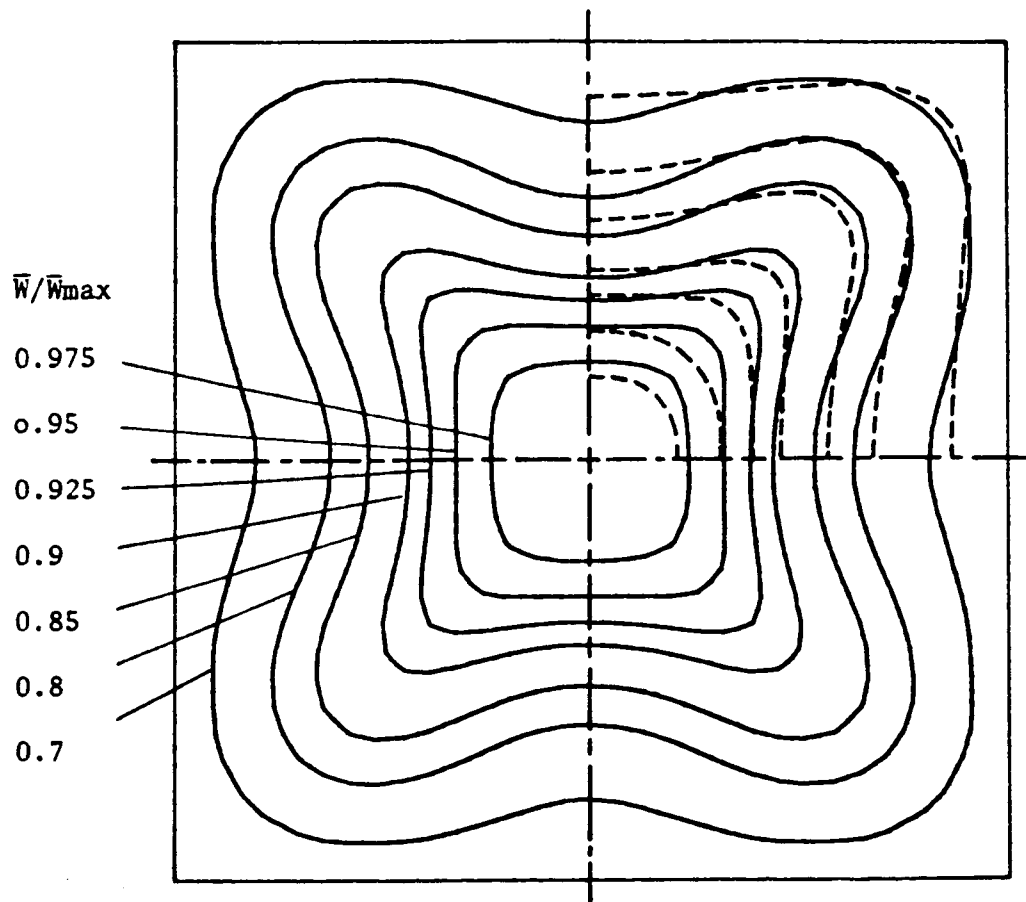
**Computational Domain with Staggered Mesh**

**Figure 4**



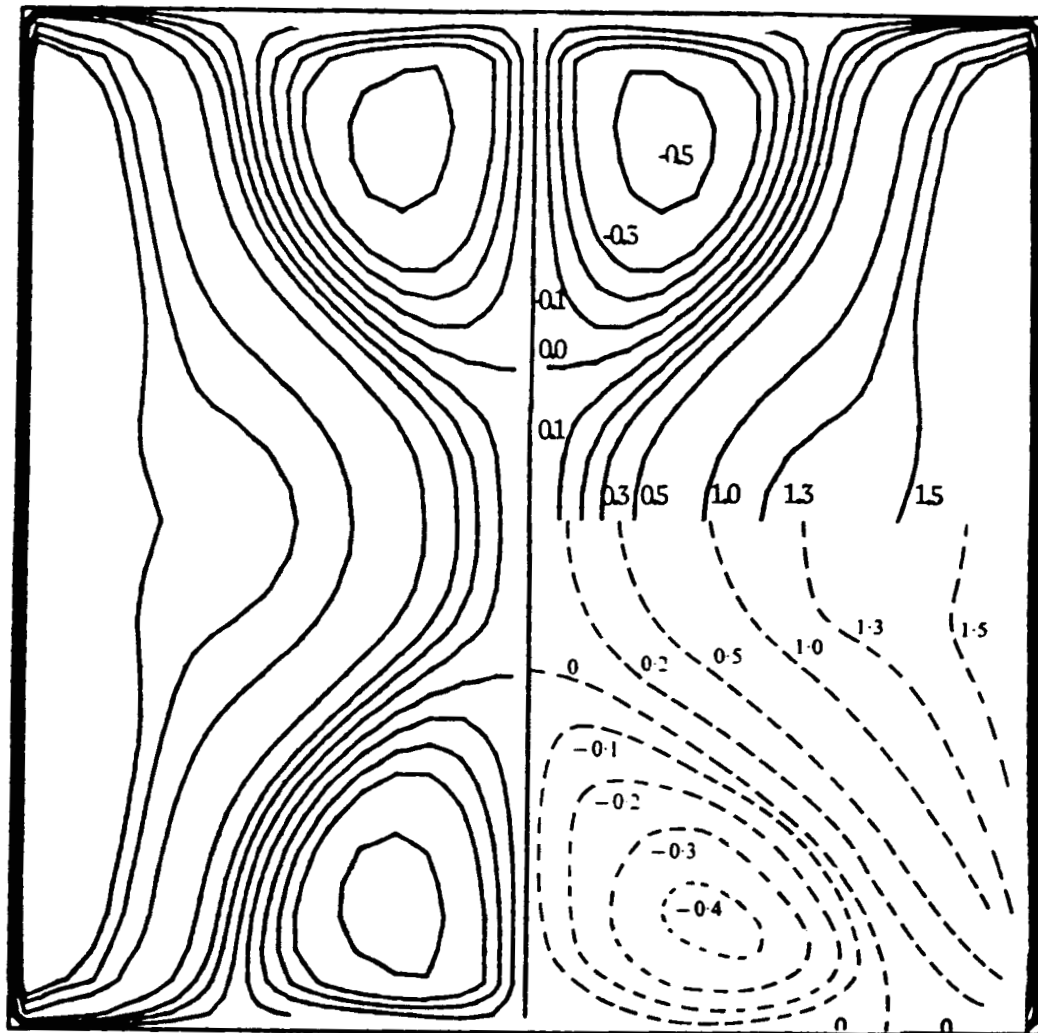
**Comparison of Fully-Developed Secondary Flow Streamlines Based on the Nonlinear K- $\epsilon$  Model in a Straight Duct at  $Re \approx 42000$  with the Experiments of Gessner & Jones [curve A:  $Re \approx 150000$ ] and the Computations of Nakayama *et al* [curve B:  $Re \approx 83000$ ]**

**Figure 5**



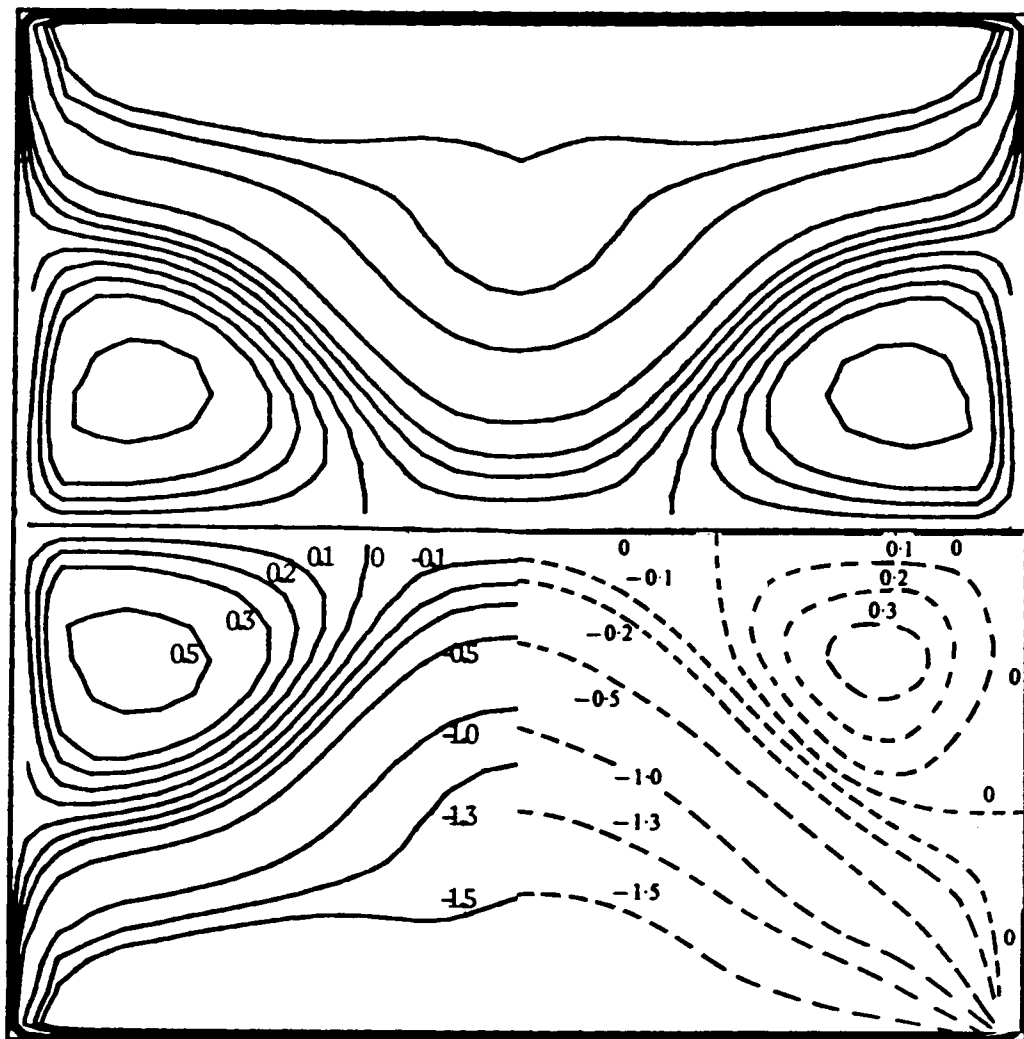
**Comparison of Azimuthal Velocity Contours ( $\bar{w}$ ) at  $Re \approx 42000$ :**  
**— Nonlinear K-1 Model; - - - Experiments of Melling & Whitelaw**

**Figure 6**



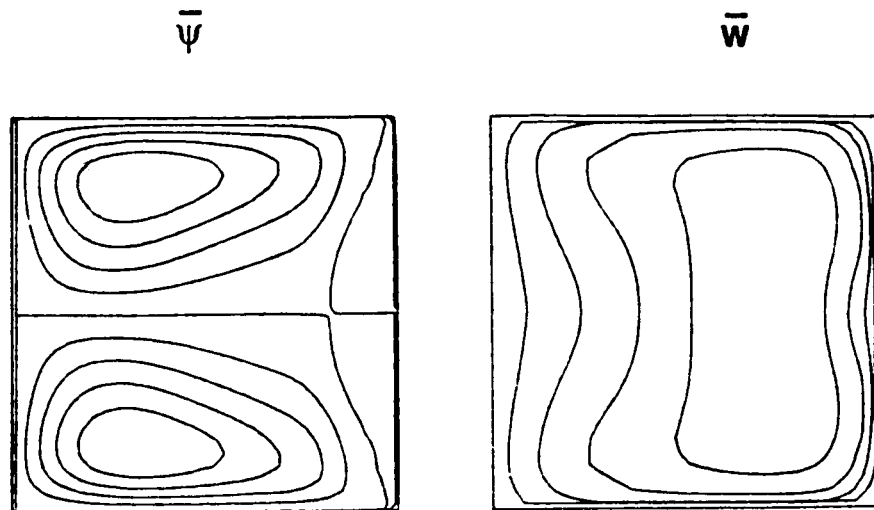
**Comparison of Reynolds Stress ( $\tau_{xz}$ ) Contours at  $Re \approx 42000$ :**  
**— Nonlinear K- $\epsilon$  Model; - - - Experiments of Melling & Whitelaw**

**Figure 7**

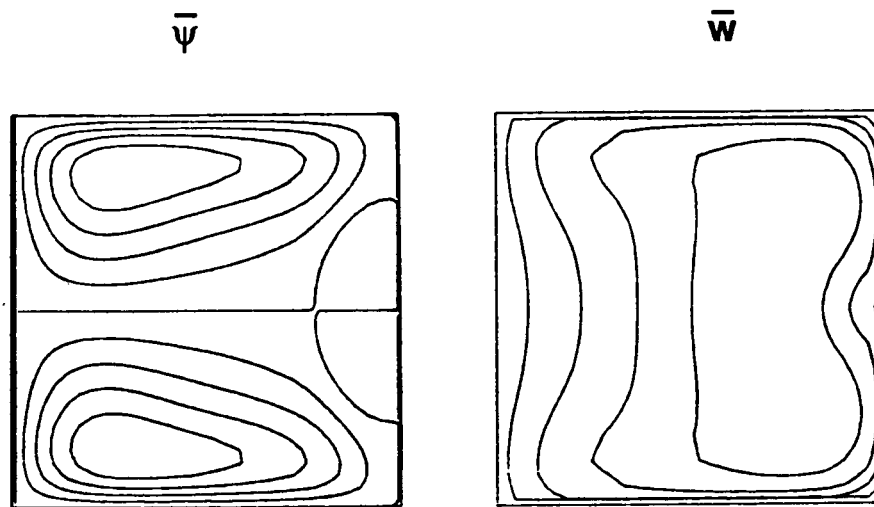


Comparison of Reynolds Stress ( $\tau_{yz}$ ) Contours at  $Re \approx 42000$ :  
 — Nonlinear K-l Model; - - - Experiments of Melling & Whitelaw

Figure 8



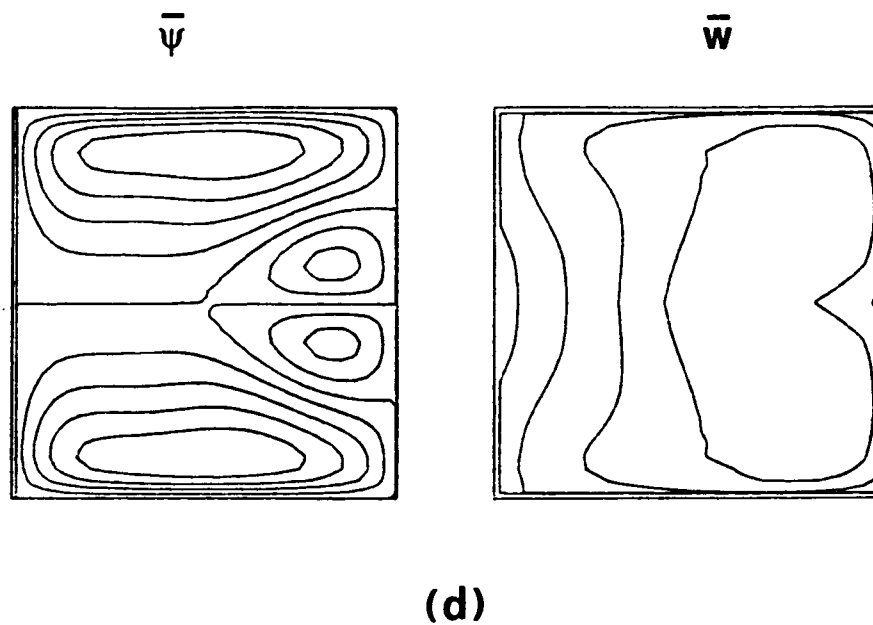
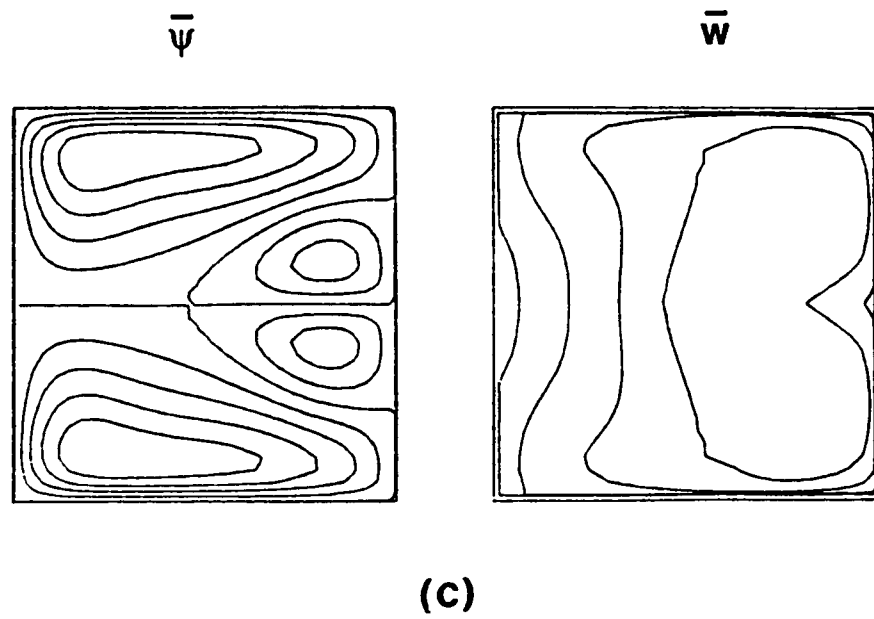
(a)



(b)

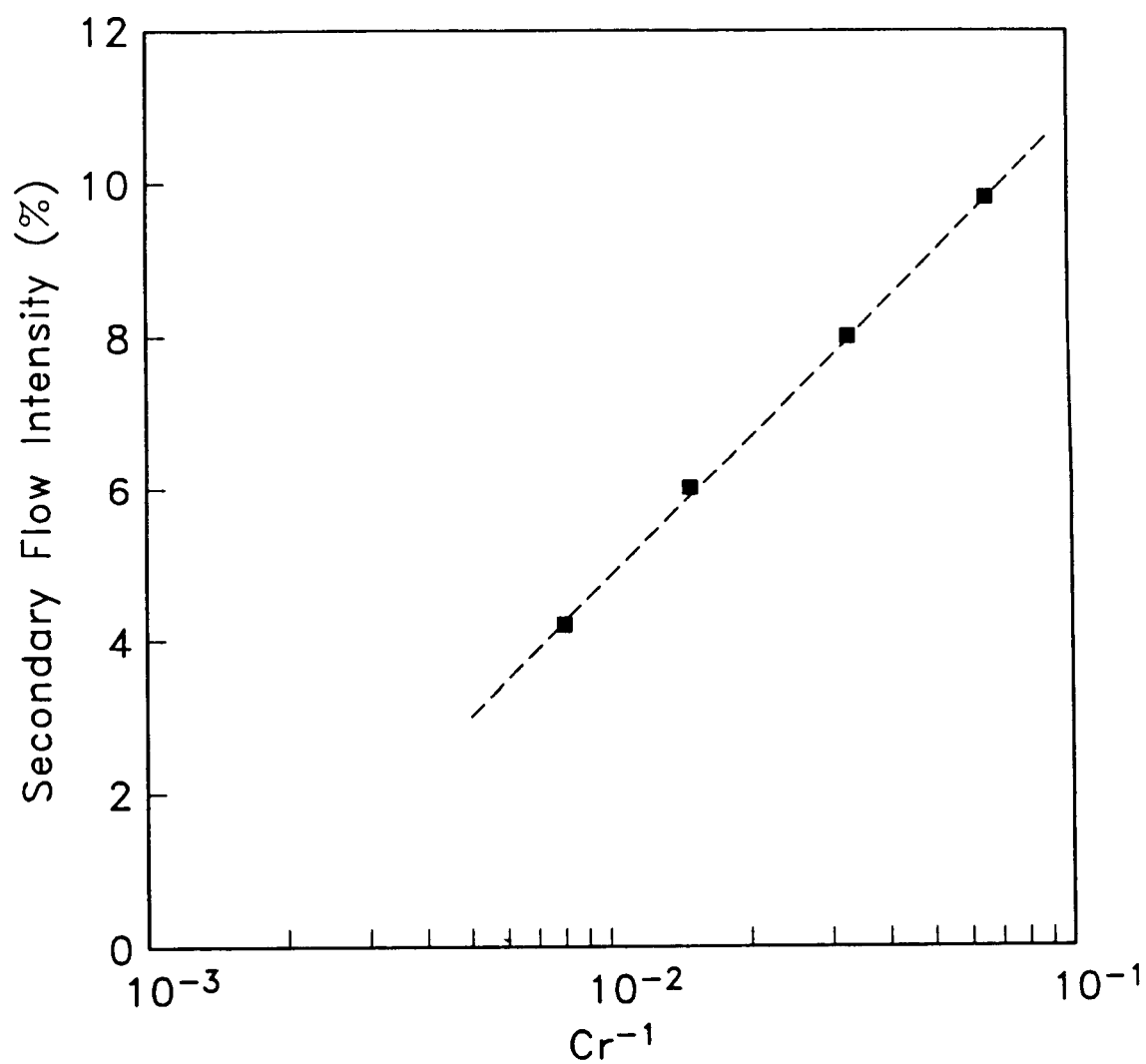
**Secondary Flow Streamlines ( $\bar{\psi}$ ) and Azimuthal Velocity ( $\bar{w}$ ) for  
Turbulent Flow in Curved Ducts at  $Re \approx 42000$   
a)  $Cr = 125$ , b)  $Cr = 62.5$ , c)  $Cr = 31.25$ , d)  $Cr = 15.63$**

**Figure 9**



**Secondary Flow Streamlines ( $\bar{\psi}$ ) and Azimuthal Velocity ( $\bar{w}$ ) for  
Turbulent Flow in Curved Ducts at  $Re \approx 42000$   
a)  $Cr = 125$ , b)  $Cr = 62.5$ , c)  $Cr = 31.25$ , d)  $Cr = 15.63$**

**Figure 9**



Effect of Curvature on Secondary Flow Intensity for Square Ducts ( $Re = 42000$ )

**Figure 10**



## Report Documentation Page

1. Report No. NASA CR-181830 ICASE Report No. 89-25		2. Government Accession No.		3. Recipient's Catalog No.	
4. Title and Subtitle NUMERICAL STUDY OF TURBULENT SECONDARY FLOWS IN CURVED DUCTS				5. Report Date April 1989	
				6. Performing Organization Code	
7. Author(s) N. Hur, S. Thangam, C. G. Speziale				8. Performing Organization Report No. 89-25	
				10. Work Unit No. 505-90-21-01	
9. Performing Organization Name and Address Institute for Computer Applications in Science and Engineering Mail Stop 132C, NASA Langley Research Center Hampton, VA 23665-5225				11. Contract or Grant No. NAS1-18605	
				13. Type of Report and Period Covered Contractor Report	
12. Sponsoring Agency Name and Address National Aeronautics and Space Administration Langley Research Center Hampton, VA 23665-5225				14. Sponsoring Agency Code	
15. Supplementary Notes Langley Technical Monitor: ASME J. Fluids Engng. Richard W. Barnwell  Final Report					
16. Abstract <p>The pressure driven, fully-developed turbulent flow of an incompressible viscous fluid in curved ducts of square cross-section is studied numerically by making use of a finite volume method. A nonlinear <math>K - \epsilon</math> model is used to represent the turbulence. The results for both straight and curved ducts are presented. For the case of fully-developed turbulent flow in straight ducts, the secondary flow is characterized by an eight-vortex structure for which the computed flowfield is shown to be in good agreement with available experimental data. The introduction of moderate curvature is shown to cause a substantial increase in the strength of the secondary flow and to change the secondary flow pattern to either a double-vortex or a four-vortex configuration.</p>					
17. Key Words (Suggested by Author(s)) turbulent flow; $K - \epsilon$ model; curved ducts			18. Distribution Statement 34 - Fluid Mechanics and Heat Transfer Unclassified - Unlimited		
19. Security Classif. (of this report) Unclassified		20. Security Classif. (of this page) Unclassified		21. No. of pages 26	22. Price A03